buildings

MDPI

Article

A Comparison of the Quasi-Steady Assumption with Unsteady Effects on Tower Galloping Analysis

Zihang Yang [1], Yangzhao Liu [1,*], Ying Chang [2] and Kaoshan Dai [1,2]

[1] Department of Civil Engineering, Sichuan University, Chengdu 610065, China
[2] Institute for Disaster Management and Reconstruction, Sichuan University-The Hong Kong Polytechnic University, Chengdu 610065, China; changying1205@scu.edu.cn
* Correspondence: liuyangzhao@scu.edu.cn

Abstract: Traditional tower galloping theory is founded on the quasi-steady assumption, which has inherent limitations. By treating tower galloping as a single-degree-of-freedom crosswind bending flutter problem and introducing flutter derivatives into the expression of the crosswind aerodynamic force acting on the tower, the unsteady effects induced by motion can be incorporated into the analysis of tower galloping. An actual chamfered square cross-section tower was used as the research subject, and static tests and flutter derivative identification tests were performed on tower segment models without any modifications and with two types of aerodynamic measures: added arc-shaped fairings and vertical fin plates. Predictions of the aerodynamic damping of the tower structure were made and compared based on two different galloping theories: one under the quasi-steady assumption and the other considering unsteady effects. Experimental results indicate that both theories lead to the same conclusion about the galloping stability of the chamfered square tower. The original cross-section tower exhibited significant galloping instability problems, but the addition of arc-shaped fairings or vertical fin plates effectively improved its galloping stability performance. The predicted results of the tower's aerodynamic damping based on the two different galloping theories differed by at most 34% at dimensionless wind speeds below 25. However, some differences were observed, and these differences between the two theories were noticeably affected by the magnitude of the dimensionless wind speed.

Keywords: tower column; galloping analysis; quasi-steady theories; unsteady effects; wind tunnel tests

Citation: Yang, Z.; Liu, Y.; Chang, Y.; Dai, K. A Comparison of the Quasi-Steady Assumption with Unsteady Effects on Tower Galloping Analysis. *Buildings* **2024**, *14*, 3707. https://doi.org/10.3390/buildings14123707

Academic Editor: Theodore Stathopoulos

Received: 5 October 2024
Revised: 28 October 2024
Accepted: 29 October 2024
Published: 21 November 2024

1. Introduction

Tower structures that are highly flexible, lightweight, and have low damping, especially those with blunt cross-sections, often exhibit poor wind resistance and are susceptible to galloping. Galloping is a divergent self-excited vibration that commonly occurs in structures with complex, irregular, non-streamlined cross-sections, such as square, rectangular, and triangular cross-sections [1–3]. At supercritical wind speeds, the amplitude of the structure can rapidly increase, resulting in galloping that is highly destructive [4]. One prominent example of galloping-induced failure is the Tacoma Narrows Bridge collapse, colloquially known as "Galloping Gertie". This highlights the need for significant attention to this phenomenon in engineering practice.

The galloping phenomenon in structures has been extensively investigated under the quasi-steady assumption by numerous researchers. Shiraishi et al. [5] investigated the fluid–structure interaction and flow-induced vibrations (FIV) in rectangular cylinders, highlighting their susceptibility to galloping instability due to symmetry and simple cross sections. Novak [6] and Parkinson and Smith [7] established the basis for understanding galloping as a single-degree-of-freedom flutter, extending Den Hartog's quasi-steady instability criterion to nonlinear systems. Nishimura [8] performed wind tunnel experiments to determine the static aerodynamic force coefficients for rectangular sections, providing

essential data for galloping analysis. Barrero-Gil et al. [9,10] mathematically analyzed how key points on the force curve influence galloping behavior. Ng et al. [11] demonstrated that a seventh-order polynomial adequately captures the galloping behavior of square cylinders, including hysteresis, supporting the use of quasi-steady theory in predicting flow-induced vibrations. Lindner [12] confirmed that the quasi-steady theory remains valid for galloping in turbulent flows for certain prism geometries, reinforcing its applicability under specific turbulent conditions. Joly et al. [13] showed that the quasi-steady model accurately predicts galloping at high mass ratios but fails at lower ratios, indicating its limitations in capturing sudden changes in oscillation amplitude. Nakamura and Tomonari [14] identified a correlation between the critical depth and the onset of soft galloping in rectangular prisms within the quasi-steady framework. Parkinson and Sullivan [15] demonstrated that incorporating sectional force variation along the height of square-section towers improves the accuracy of quasi-steady galloping predictions. Ruscheweyh et al. [16] developed a model to predict galloping and vortex-induced vibrations, validated through full-scale tests, providing better prediction parameters within the quasi-steady theory for practical engineering use. Santosham [17] compared experimental results from wind tunnel tests on rectangular cylinders with predictions of quasi-steady theory, supplying data for evaluating theoretical models. Brooks [18] observed that rectangular cylinders with higher aspect ratios experience galloping, while lower ratios tend toward vortex resonance, contributing to the understanding of these behaviors under the quasi-steady assumption. Novak and Tanaka [19] extended quasi-steady galloping theory to include drag-induced variations in the angle of attack, finding that turbulence significantly increases galloping tendencies in D-sections and rectangular sections. Parkinson and Wawzonek [20] examined the interaction between galloping and vortex resonance in towers, highlighting the limitations of the quasi-steady theory. Jones [21] examined the coupled vertical and horizontal galloping of iced conductors, providing equations that clarify the interaction between these motion types under the quasi-steady assumption. Robertson et al. [22] conducted numerical simulations on rectangular cross-sections with various length-to-width ratios to determine the galloping tendencies of specific rectangular prisms.

However, several studies have highlighted the limitations of the quasi-steady assumption and emphasized the importance of considering unsteady effects in galloping analysis. Abdel-Rohman [23] developed a model incorporating unsteady wind effects in galloping analysis, underscoring the limitations of the quasi-steady assumption in dynamic stability predictions. Gao et al. [24] proposed a nonlinear unsteady galloping model, demonstrating the critical role of unsteady aerodynamic damping in predicting instability at low wind speeds, thus advancing beyond the quasi-steady framework. Mannini et al. [25–28] investigated unsteady galloping phenomena, identifying unsteady galloping in turbulent flows and challenging the quasi-steady theory's applicability under such conditions. Their experiments demonstrated the limitations of the quasi-steady approach in predicting galloping instability due to vortex shedding interaction and unsteady aerodynamic forces. Liu et al. [29] proposed a novel time-varying flow pattern approach to enhance the understanding of transverse galloping in rectangular cylinders through unsteady analysis. Sourav et al. [30] measured the transitional mass ratio at the onset of galloping for square cross-section columns at a minimum Reynolds number of 150, emphasizing unsteady effects at low Reynolds numbers. Claudia et al. [31] presented a method for structural galloping stability analysis that incorporates nonlinear aerodynamic damping, highlighting the significance of unsteady aerodynamic forces in predicting galloping instability.

Furthermore, some researchers have explored both quasi-steady and unsteady aspects to provide a more comprehensive understanding of galloping mechanisms. Barrero-Gil et al. [32] investigated galloping at low Reynolds numbers, identifying limitations in the quasi-steady hypothesis—particularly when hysteresis is absent—and suggesting the need for unsteady approaches. Borri et al. [33] showed that when VIV and galloping critical velocities are close, a distinct vibration pattern emerges, highlighting the complexity in predicting interactions between these phenomena and the necessity of incorporating both

quasi-steady and unsteady theories. Corless and Parkinson [34] combined models for VIV and galloping, revealing nonlinearities that occur when both oscillations coexist, thereby improving predictions of structural response by integrating both theoretical approaches. Tian et al. [35] applied numerical simulations to complex systems such as multi-span iced eight-bundle conductors. Their analysis demonstrated how variations in span length, wind velocity, and conductor configuration affect the dynamic response of these systems, underscoring the importance of considering both quasi-steady and unsteady effects to accurately predict structural stability under wind loads.

Most existing analyses of tower galloping are based on the quasi-steady assumption [36], in which aerodynamic forces are considered quasi-steady. This means that the crosswind aerodynamic forces acting on the tower depend only on the instantaneous relative velocity between the incoming flow and the structure, as well as the wind angle relative to the structure. However, airflow around a vibrating structure generates unsteady aerodynamic forces, even when the incoming flow is uniform, and the structural cross-section is ideally streamlined. Therefore, relying exclusively on quasi-steady effects to analyze tower galloping can result in discrepancies between theory and practice. Incorporating unsteady effects into traditional quasi-steady theoretical calculations is essential for resolving this type of galloping problem. In this study, flutter derivatives obtained from wind tunnel experiments are incorporated into the calculation of the tower's crosswind aerodynamic forces, allowing the galloping analysis to include unsteady effects (broadly speaking, unsteady aerodynamic forces include motion-induced self-excited forces, turbulence-induced buffeting forces, vortex-induced forces, etc.; here, the focus is specifically on self-excited forces in uniform flow, i.e., unsteady effects induced by motion). An actual tower structure is employed as an example to comprehensively compare the similarities and differences between two theoretical analysis methods and experimental results for tower galloping—one based on the quasi-steady assumption and the other including unsteady effects.

2. Two Theories of Tower Galloping Based on the Quasi-Steady Assumption and Considering Unsteady Effects

2.1. Tower Galloping Theory Based on the Quasi-Steady Assumption

Den Hartog [36] first explained transverse galloping using a linearized quasi-steady instability criterion, laying the foundation for future studies. Later, Parkinson and Smith [7] extended this criterion to a nonlinear differential equation with a small damping term, allowing theoretical predictions of post-critical behaviors in elastic systems. Quasi-steady theory uses static force coefficients from a fixed (non-vibrating) body to estimate aerodynamic excitations on a vibrating structure, effectively capturing the response of structures like square cylinders under crosswind conditions.

2.1.1. Quasi-Steady Aerodynamic Forces in the Crosswind Direction

As depicted in Figure 1a, a uniform flow with velocity v flows perpendicularly (wind angle is zero) over a slender tower structure. The tower itself experiences slight vibrations in the crosswind direction (the Y-direction perpendicular to the incoming flow in the figure) with a velocity $\dot{y}$.

Applying the principle of relative motion, the tower is considered stationary, and the incoming wind is viewed as flowing over this "stationary" tower with a relative wind angle α and a relative velocity v_α. As depicted in Figure 1b, α and v_α are expressed as:

$$\alpha = \arctan(\dot{y}/v), v_\alpha = \sqrt{v^2 + (\dot{y})^2} \tag{1}$$

Under these conditions, as illustrated in Figure 1c, the incoming wind generates a drag force $F_D(\alpha)$ and a lift force $F_L(\alpha)$ per unit length on the tower, given by:

$$\begin{cases} F_D(\alpha) = \frac{1}{2}\rho v_\alpha^2 B C_D(\alpha) \\ F_L(\alpha) = \frac{1}{2}\rho v_\alpha^2 B C_L(\alpha) \end{cases} \tag{2}$$

where $C_D(\alpha), C_L(\alpha)$ are the drag and lift coefficients of the tower in the wind-axis coordinate system, both based on the tower's crosswind width B as the characteristic dimension.

The net aerodynamic force acting on the tower in the Y-direction, derived by combining the projections of the drag force $F_D(\alpha)$ and the lift force $F_L(\alpha)$, is the crosswind quasi-steady aerodynamic force:

$$F_y(\alpha) = -[F_D(\alpha)\sin\alpha + F_L(\alpha)\cos(\alpha)] = -\frac{1}{2}\rho v^2 B C_{Fy}(\alpha) \tag{3}$$

where $C_{Fy}(\alpha) = (C_L + C_D\tan\alpha)\sec\alpha$.

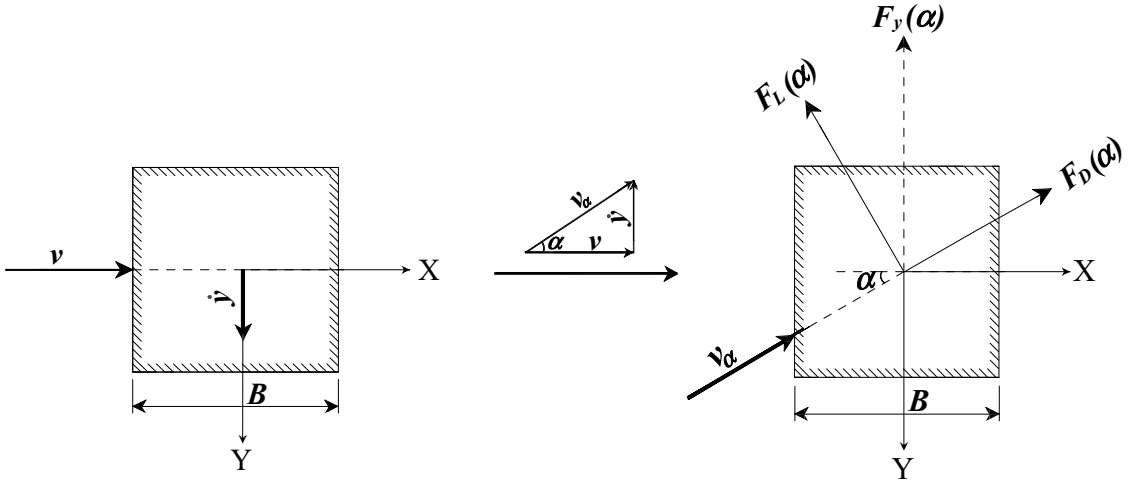

(**a**) Uniform wind flowing perpendicularly over a slightly vibrating tower

(**b**) Equivalent transformation of relative motion

(**c**) Uniform wind flowing over an effectively stationary tower

Figure 1. Schematic diagram of the crosswind aerodynamic force on the tower column based on quasi-steady theories.

2.1.2. Equation of Motion in the Crosswind Direction

With the expression for the crosswind aerodynamic force established, the tower's vibration equation in the crosswind direction can be readily derived using structural dynamics principles:

$$m\ddot{y} + 2m\zeta\omega\dot{y} + m\omega^2 y = F_y(\alpha) \tag{4}$$

where y represents the crosswind displacement of the tower, and m, ζ, and ω denote the equivalent mass, damping coefficient, and stiffness corresponding to the tower's crosswind vibration mode.

Assuming slight tower vibrations, $\alpha \approx \dot{y}/v \to 0$ is approximated. F_y is expanded around $\alpha = 0$ using a first-order Taylor series:

$$F_y(\alpha) = F_y(0) + \frac{\partial F_y}{\partial \alpha}|_{\alpha=0}\alpha + \Delta(\alpha^2) \tag{5}$$

where, $F_y(0)$ is a constant term that does not vary with time and can be neglected in dynamic response analysis; the term $\Delta(\alpha^2)$ represents the linear terms of α^2 in the aerodynamic force, with higher-order terms neglected. Therefore, $F_y(\alpha)$ simplifies to:

$$F_y(\alpha) \approx \frac{\partial F_y}{\partial \alpha}|_{\alpha=0}\alpha \tag{6}$$

Differentiating Equation (3) with respect to F_y yields the expression for the crosswind quasi-steady aerodynamic force:

$$F_y(\alpha) = -\frac{1}{2}\rho v B(\frac{dC_L}{d_\alpha} + C_D)\dot{y} \tag{7}$$

By substituting Equation (7) into Equation (4) and rearranging terms, the crosswind vibration equation of the tower is obtained:

$$m\ddot{y} + \left[2m\zeta\omega + \frac{1}{2}\rho v B(\frac{dC_L}{d_\alpha} + C_D)\right]\dot{y} + m\omega^2 y = 0 \tag{8}$$

2.1.3. Criteria for Galloping Stability and the Critical Wind Speed at Which Galloping Occurs

The preceding equation aligns with the form of the free vibration equation for a single-degree-of-freedom system. The coefficient preceding the velocity term $\dot{y}$ represents the net damping of the tower system—that is, the sum of the tower's mechanical damping and aerodynamic damping—denoted as d_s:

$$d_s = 2m\zeta\omega + \frac{1}{2}\rho v B s \tag{9}$$

$$s = \frac{dC_L}{d\alpha} + C_D \tag{10}$$

where s is referred to as the galloping coefficient. If $s \geq 0$, then net damping $d_s > 0$, indicating that the tower's vibrations will decay, and galloping divergence will not occur. Only when $s < 0$ can the net damping become negative ($d_s < 0$), leading to potential divergent galloping instability in the tower. Therefore, having $s < 0$ is a necessary condition for galloping instability to occur in the tower.

When the system's net damping $d_s = 0$, the tower enters an undamped, constant-amplitude vibration state, known as the critical state of galloping. At this point, using Equation (9), the expression for the tower's critical galloping wind speed based on the quasi-steady assumption is derived:

$$v_c^s = -\frac{4m\zeta\omega}{\rho s B} \tag{11}$$

Analyzing the expression for the critical galloping wind speed v_c^s, it can be observed that a smaller negative value of s (indicating a larger absolute value), leads to a lower v_c^s, increasing the likelihood of galloping and indicating poorer tower stability. Conversely, a larger negative value of s (i.e., the smaller its absolute value), improves the tower's galloping stability.

2.2. Tower Galloping Theory Incorporating Unsteady Effects

In Section 2.1, the crosswind aerodynamic force on the tower was assumed to rely solely on the instantaneous relative velocity between the incoming flow and the structure, as well as the wind angle relative to the structure. Theoretically, the tower's galloping may be modeled as a single-degree-of-freedom flutter problem involving lateral bending in the crosswind direction. A uniform flow around a vibrating tower will generate unsteady aerodynamic forces on the structure. Solely relying on quasi-steady factors in galloping theory can cause discrepancies between theory and practice, thus making it crucial to incorporate unsteady effects into galloping analysis.

2.2.1. Unsteady Aerodynamic Forces in the Crosswind Direction

In calculating the flutter response of bridge structures, Scanlan [37] formulated the unsteady aerodynamic forces acting on the main girder (as depicted in Figure 2a) as:

$$\begin{cases} \mathrm{L} = \frac{1}{2}\rho v^2(2B)\left[KH_1^*\frac{\dot{h}}{v} + KH_2^*\frac{\dot{\alpha}B}{v} + K^2H_3^*\alpha + K^2H_4^*\frac{h}{B}\right] \\ \mathrm{M} = \frac{1}{2}\rho v^2\left(2B^2\right)\left[KA_1^*\frac{\dot{h}}{v} + KA_2^*\frac{\dot{\alpha}B}{v} + K^2A_3^*\alpha + K^2A_4^*\frac{h}{B}\right] \end{cases} \quad (12)$$

where L and M represent the aerodynamic lift and moment per unit length acting on the main girder. h, $\dot{h}$ are the vertical displacement and velocity, and α, $\dot{\alpha}$ are the torsional angle and angular velocity of the main girder's vibration. B is the main girder's width. ρ is the air density (=1.225 kg/m^3). v is the wind speed. K is the dimensionless reduced frequency defined as $K = \omega B/v$, with ω being the natural circular frequency of vibration. The coefficients H_i^*, A_i^*, $(i = 1, 2, 3, 4)$ are dimensionless and dependent on K, known as flutter derivatives or aerodynamic derivatives, which are determined through wind tunnel tests on sectional models of the main girder.

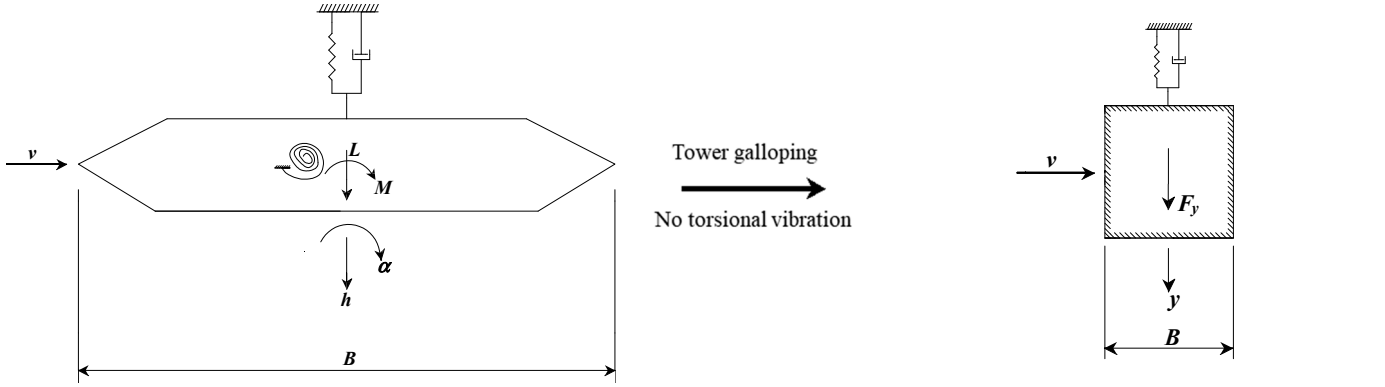

(**a**) Two-degree-of-freedom wind-induced vibration model of the main girder considering vertical bending and torsion

(**b**) Single-degree-of-freedom lateral bending wind-induced vibration model of the tower

Figure 2. Schematic diagram of the crosswind aerodynamic force on the tower column taking account of unsteady effects.

By treating the tower's galloping as a specific case of a flutter problem involving only crosswind lateral bending vibration, Scanlan's unsteady aerodynamic force expressions can be applied to the tower's galloping analysis. In this case, the tower experiences only crosswind aerodynamic forces F_y (see Figure 2b) without aerodynamic moments. Additionally, the tower's crosswind aerodynamic force is essentially equivalent to the aerodynamic lift L acting on the main girder and can be represented using the same formulas (see Equation (12)). Since the tower does not undergo torsional vibration, the torsional angle and angular velocity are zero, eliminating the terms involving $(\alpha, \dot{\alpha})$ in the aerodynamic force expressions. As a result, the tower's crosswind aerodynamic force F_y simplifies to:

$$\mathrm{F}_y = \frac{1}{2}\rho v^2(2B)\left[KH_1^*\frac{\dot{y}}{v} + 0KH_2^*\frac{B}{v} + 0K^2H_3^* + K^2H_4^*\frac{y}{B}\right] = \frac{1}{2}\rho v^2(2B)\left[KH_1^*\frac{\dot{y}}{v} + K^2H_4^*\frac{y}{B}\right] \quad (13)$$

where, y and $\dot{y}$ represent the displacement and velocity of the tower's crosswind vibration, analogous to those in the main girder's aerodynamic force expressions. B denotes the tower's characteristic width in the crosswind direction; all other symbols retain the same meanings as in Equation (12).

2.2.2. Crosswind Vibration Equation

With the expression for the tower's crosswind unsteady aerodynamic force F_y established, the crosswind vibration equation accounting for unsteady effects can be readily formulated:

$$m\ddot{y} + 2m\zeta\omega\dot{y} + m\omega^2 y = F_y = \frac{1}{2}\rho v^2(2B)\left[KH_1^*\frac{\dot{y}}{v} + K^2H_4^*\frac{y}{B}\right] \tag{14}$$

Bringing the right-hand term to the left side, the equation becomes:

$$m\ddot{y} + \left[2m\zeta\omega - \frac{1}{2}\rho v^2(2B)KH_1^*\frac{1}{v}\right]\dot{h} + \left[m\omega^2 - K^2H_4^*\frac{1}{B}\right]h = 0 \tag{15}$$

This equation aligns with the form of a single-degree-of-freedom free vibration equation. The combined mechanical and aerodynamic damping preceding the velocity term $\dot{y}$ represent the net damping of the tower system when unsteady effects are considered, denoted as d_u, specifically:

$$d_u = 2m\zeta\omega - \frac{1}{2}\rho v^2(2B)KH_1^*\frac{1}{v} \tag{16}$$

2.2.3. Galloping Stability Criterion and Critical Wind Speed

The tower's galloping stability is assessed using the expression of net damping d_u in Equation (16) when unsteady effects are included: if $H_1^* \leq 0$, it ensures that $d_u > 0$, indicating that galloping instability of the tower will not occur. Only when $H_1^* > 0$ can the net damping become negative $d_u < 0$, leading to possible divergent vibrations in the tower. Therefore, $H_1^* > 0$ is the necessary condition for crosswind galloping instability of the tower when unsteady effects are considered. When $d_u = 0$, the tower's structural response shifts from stable to divergent, allowing for the determination of H_1^* at the critical galloping state:

$$H_1^* = \frac{2m\zeta}{\rho B^2} \tag{17}$$

Through wind tunnel tests, the variation curve of H_1^* with the dimensionless wind speed V_* for the tower cross-section can be obtained. The dimensionless wind speed is defined as:

$$V_* = \frac{v}{fB} \tag{18}$$

where f denotes the natural frequency of the tower's crosswind vibration. v and B retain their previous meanings, representing the actual wind speed and the tower's characteristic crosswind width, respectively.

Using the tower's H_1^*-V_* curve, the critical dimensionless wind speed V_{*c} at which Equation (17) applies can be determined. Correspondingly, the critical galloping wind speed is:

$$v_c^u = fBV_{*c} \tag{19}$$

This is the formula for calculating the tower's crosswind critical galloping wind speed when unsteady effects are included.

3. Static Tests and Flutter Derivative Identification Using a Chamfered Square Tower Segment Model

The study is based on a single-column chamfered square cross-section tower from a large-span cable-stayed bridge. A tower segment model was fabricated based on the typical upper tower cross-section, scaled geometrically according to a specified ratio (1:30), the model features a square cross-section with four symmetrical straight chamfers, both the width and height of the model are equal, denoted as B = 0.1365 m, and the chamfer width is denoted as L = 2.095 m, as illustrated in Figure 3 [38]. The static and flutter derivative

identification tests of the tower segment model were carried out in the second test section of the XNJD-1 industrial wind tunnel at Southwest Jiaotong University; this test section features a rectangular cross-section measuring 2.4 m in width and 2.0 m in height. It is equipped with sidewall supports and a force balance system designed for static testing of segment models, along with a spring suspension device for flutter derivative identification. The experiments were conducted using only uniform flow fields. Figure 4 displays the segment model mounted on the wind tunnel's support system.

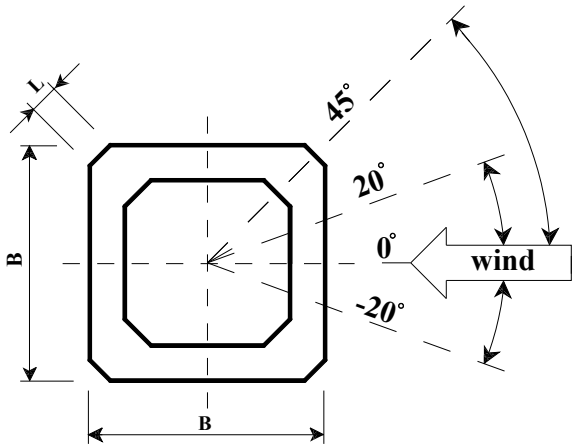

Figure 3. Cross-section drawing of sectional model for the tower column and definition of wind direction in tests.

Figure 4. Section model suspended in wind tunnel.

3.1. Static Tests on the Tower Segment Model

3.1.1. Segment Model Without Modifications

Initially, static tests were performed on the tower segment model over a wind direction angle range of 0° to 45°, in increments of 1°. The wind direction angle α is defined as illustrated in Figure 3: when the incoming wind is perpendicular to the right-angle side of the chamfered square cross-section, it is defined as a 0° wind direction angle. When the wind is perpendicular to the chamfered side of the cross-section, it is defined as a 45° wind direction angle. Utilizing the wind tunnel's force balance equipment, the average drag $F_D(\alpha)$ and lift $F_L(\alpha)$ per unit length were measured for each wind direction angle, allowing for the calculation of the tower's drag coefficient $C_D(\alpha)$ and lift coefficient $C_L(\alpha)$ using Equation (18):

$$C_D(\alpha) = F_D/(\frac{1}{2}\rho v^2 B) \tag{20}$$

$$C_L(\alpha) = F_L/(\frac{1}{2}\rho v^2 B) \tag{21}$$

where ρ = air density (=1.225 kg/m^3); B = 0.1365 m is the characteristic dimension of the sectional model; and v = wind speed experienced at the model position, which remained at a constant value of 15 m/s throughout the static force measurements, resulting in a Reynolds number of 1.37×10^5.

Figure 5 presents the variation curves of C_D and C_L for the chamfered square tower across wind direction angles from 0° to 45°. It is observed that the tower's C_D exhibits minimal fluctuation with varying wind direction angles. The C_L shows a positive slope between 6° and 45° wind direction angles, whereas an evident negative slope is present between 0° and 6°, which adversely affects the structure's galloping stability.

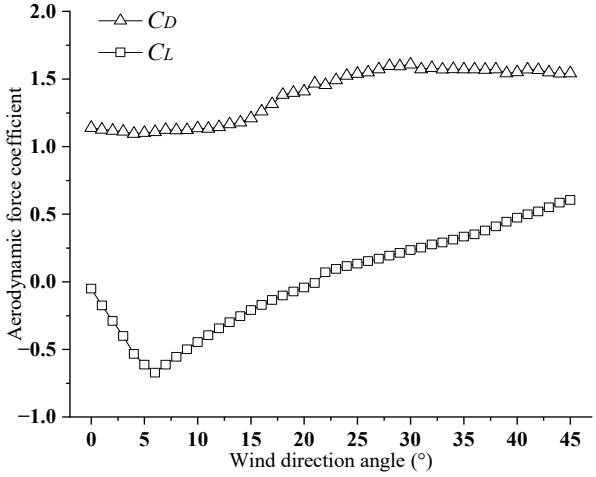

Figure 5. Test results of aerodynamic force coefficients for the tower column.

Having obtained the tower's C_D and C_L values at each wind direction angle, the galloping coefficient s versus wind direction angle is plotted using Equation (10) (see Figure 6). It is observed that the tower's galloping coefficient s remains positive between 6° and 45° and becomes negative between 0° and 5°. Therefore, based on the quasi-steady galloping stability criterion, the chamfered square tower under study may experience galloping instability between 0° and 5° wind direction angles. Additionally, the s value reaches its minimum at 0°, approximately −5.6, indicating that the tower exhibits the poorest galloping stability under a 0° wind direction.

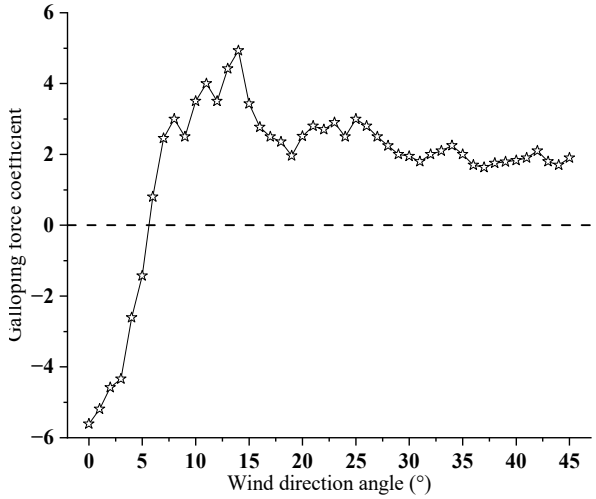

Figure 6. Test results of galloping coefficients for the tower column.

3.1.2. Segment Model Incorporating Aerodynamic Modifications

By installing arc-shaped fairings with radius R equal to the chamfer width L ($R = L$) or vertical fin plates with height $h = L$ and thickness $b = L/10$ on the four chamfered surfaces of the chamfered square tower (see Figure 7), static tests were conducted on the tower segment model with these two aerodynamic modifications. These are common aerodynamic measures that are also easy to install. Test results (Figure 8) indicate that adding arc-shaped fairings reduces the drag coefficient C_D, whereas adding vertical fin plates increases C_D. Nevertheless, both aerodynamic modifications effectively reduce the descending trend of the lift coefficient C_L in the negative slope region (i.e., they increase the negative value of $dC_L/(d\alpha)$).

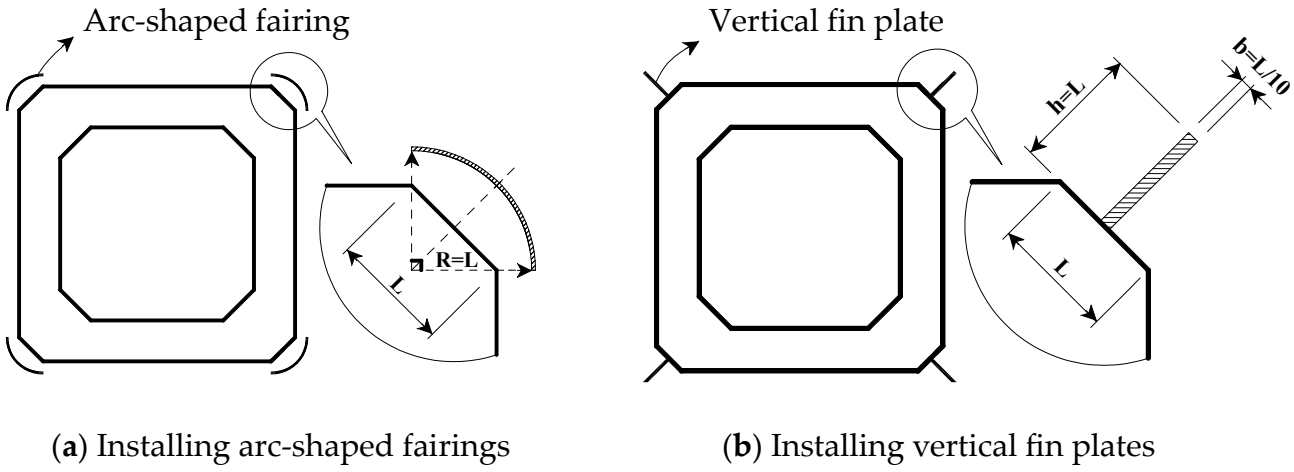

Figure 7. Sketch map of aerodynamic modifications.

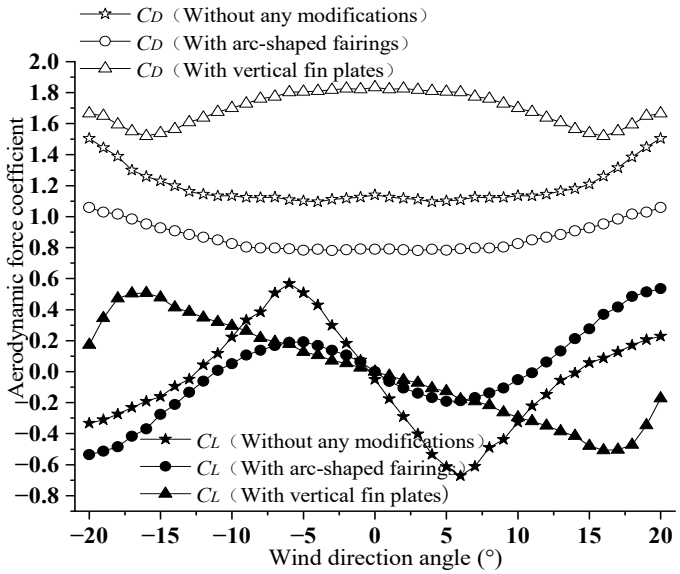

Figure 8. Comparison of aerodynamic force coefficients for the tower column before and after installing aerodynamic modifications.

Using the aerodynamic coefficient test results, a comparison of the tower's galloping coefficient s before and after installing aerodynamic modifications was made (Figure 9). It was observed that both arc-shaped fairings and vertical fin plates effectively increase the s values in the −5–5° wind angle range where the chamfered square tower is prone to galloping instability (i.e., s < 0). The improvement is particularly notable at the most critical wind angle of 0°, where the s value increases from approximately −5.6 (without any mea-

sures) to about −2.8 with arc-shaped fairings and about −1.3 with vertical fin plates. Based on the galloping stability criterion and the critical galloping wind speed formula under the quasi-steady assumption, it can be concluded that both aerodynamic measures—the arc-shaped fairings and vertical fin plates—effectively enhance the galloping stability of the chamfered square tower, particularly by significantly increasing the critical galloping wind speed at the most adverse wind angle of 0°.

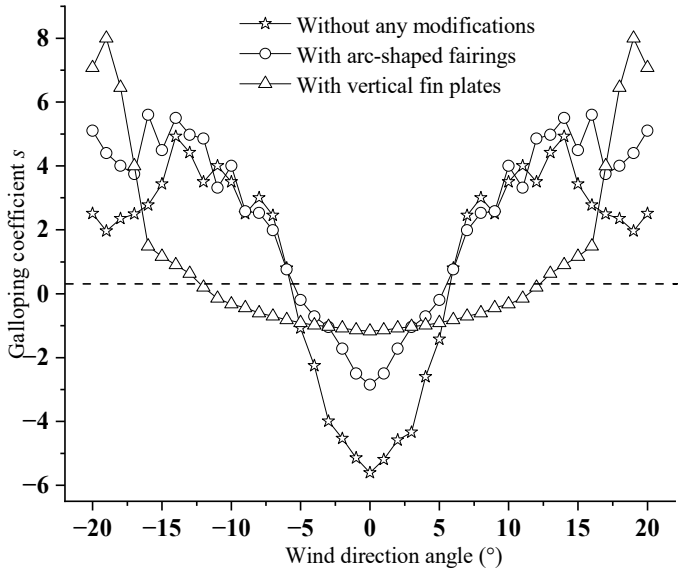

Figure 9. Comparison of galloping coefficients for the tower column before and after installing aerodynamic modifications.

3.2. Flutter Derivative Identification for the Tower Segment Model

3.2.1. Segment Model Without Modifications

To further analyze the galloping performance of the chamfered square tower using the unsteady galloping theory, additional flutter derivative identification tests were performed. The experiments were carried out at the most critical wind angle of 0°, employing the free vibration time-domain identification method. Thin strings were attached to the end plates on both sides of the tower segment model and extended outside the wind tunnel walls. For each given wind speed, an initial displacement was imparted to the tower model via the strings, which was then released to allow pure vertical free vibration. Sensors mounted on the springs recorded the free decay response of the vertical bending motion. Figure 10 presents the decay time-history curves of the model system at test wind speeds of 0 m/s, 3.08 m/s, 9.95 m/s, and 15.2 m/s. The modal damping ratio of the system evidently changes with increasing wind speed, displaying a trend of initially decreasing and then increasing.

Figure 11 shows the H_1^*-V_* curve of the chamfered square tower without any aerodynamic measures at a 0° wind direction angle. It is found that H_1^* exhibits a "negative to positive" change trend with increasing dimensionless wind speed V_*: when V_* is small and $H_1^* < 0$, the galloping stability criterion accounting for unsteady effects indicates that the tower will not experience divergent vibrations. Beyond $V_* > 7$, H_1^* becomes positive and increases significantly as V_* increases. This indicates that aerodynamic damping begins to negatively impact the net damping of the tower system. When H_1^* surpasses a certain critical positive value, the net damping becomes negative, leading to divergent crosswind vibrations of the tower, i.e., entering a galloping state.

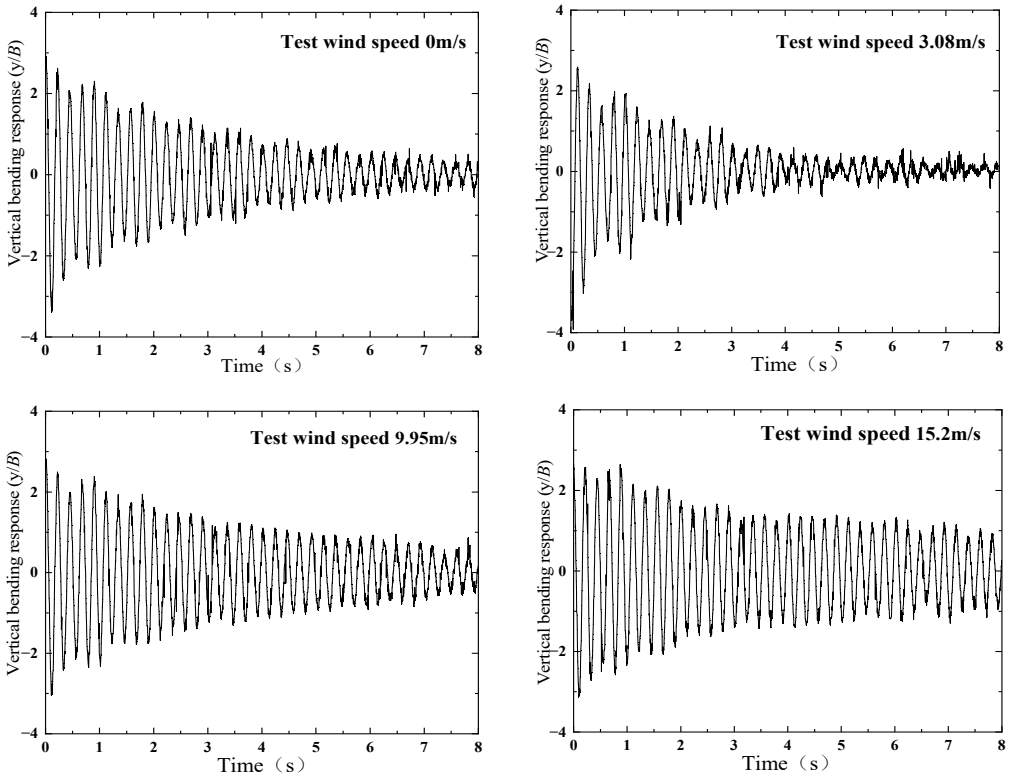

Figure 10. Vertically free vibration decay curves of the sectional model system under different test wind speeds.

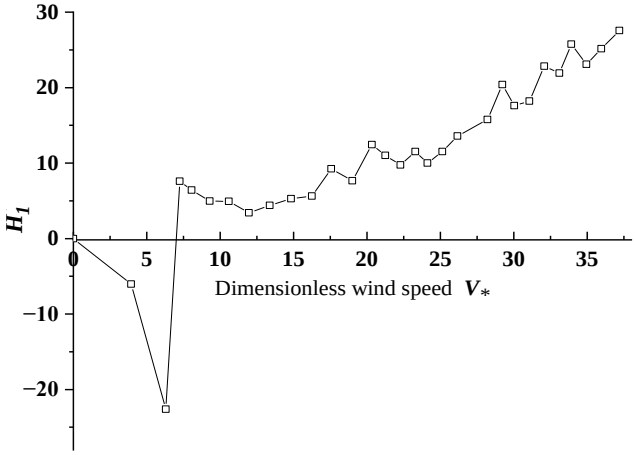

Figure 11. Flutter derivative H_1^* versus reduced wind speed for the tower column without taking any measures.

3.2.2. Segment Model with Aerodynamic Modifications

Arc-shaped fairings or vertical fin plates (see Figure 7) were installed on the four chamfered surfaces of the tower, and flutter derivative identification tests were performed under a 0° wind angle after implementing these two aerodynamic modifications. The results (Figure 12) show that, after applying aerodynamic modifications, the tower's H_1^* still displays an overall trend of transitioning from negative to positive and decreasing then increasing with increasing V_*, similar to the tower without modifications; however, both the arc-shaped fairings and vertical fin plates significantly mitigated the increasing trend of H_1^* in the positive region, effectively raising the dimensionless wind speed V_* at which divergent vibrations occur, thereby notably increasing the tower's critical galloping wind speed at a 0° wind angle.

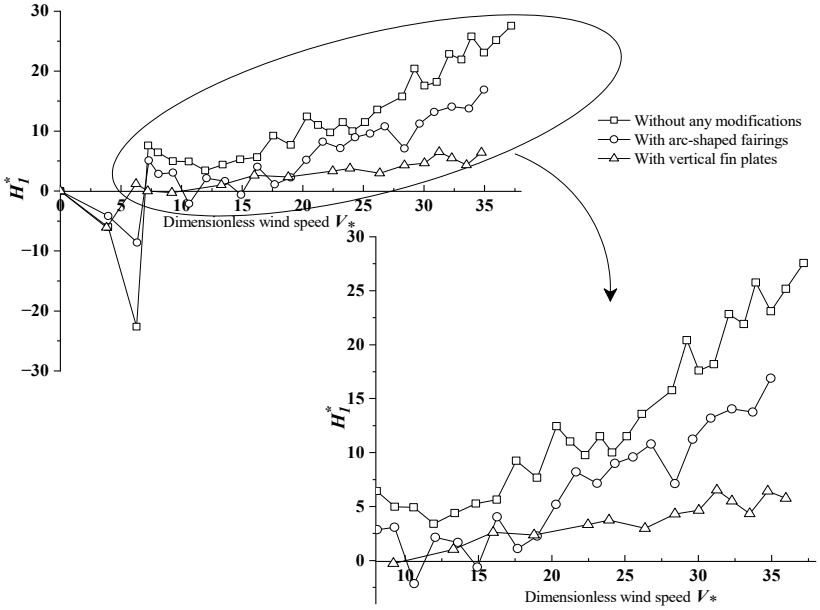

Figure 12. Comparison of flutter derivative H_1^* versus reduced wind speed with and without aerodynamic measures.

To more clearly demonstrate the crosswind bending vibration characteristics of the chamfered square tower before and after the two aerodynamic modifications, the variation curves of the tower segment model system's crosswind damping ratio with dimensionless wind speed under a 0° wind angle were plotted (Figure 13). It is observed that, without any modifications, the damping ratio of the tower model system decreases rapidly with increasing V_*, approaching zero (the system's inherent mechanical damping prevents the total damping ratio from reaching zero or negative values), indicating that the crosswind bending vibration of the chamfered square tower rapidly approaches the divergent critical state with increasing wind speed. However, it was found that adding arc-shaped fairings or vertical fin plates significantly mitigated the decreasing trend of the tower model system's crosswind bending damping ratio, further confirming that both aerodynamic modifications effectively raise the critical wind speed at which the tower enters divergent crosswind bending vibrations.

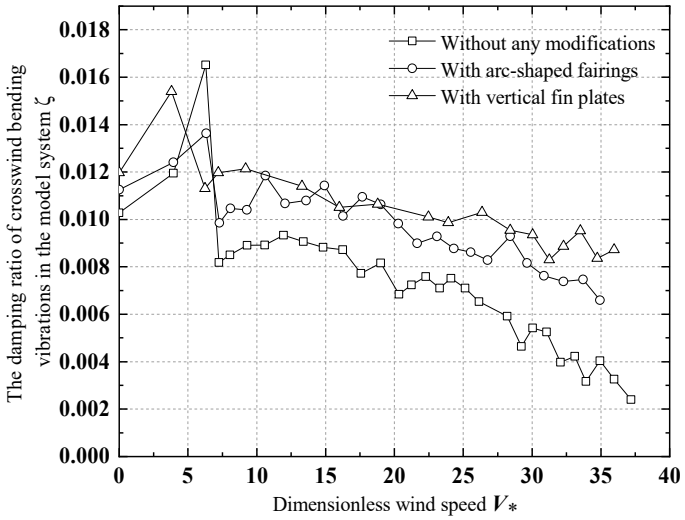

Figure 13. Crosswind bending damp ratio of the sectional model system versus reduced wind speed.

4. Comparison of Experimental Results Based on Two Different Galloping Theories for the Tower

From the preceding analysis, it is evident that determining the total apparent damping of the tower structure is critical in both the quasi-steady assumption-based and unsteady effect-inclusive galloping theories, as it influences the assessment of the tower's galloping stability and the calculation of the critical galloping wind speed. The apparent damping primarily includes two components: the tower system's inherent mechanical damping and the aerodynamic damping induced by the incoming wind. Mechanical damping is an intrinsic characteristic of the tower structure and is a known constant. The main difference between the two theories lies in their predictions of the crosswind aerodynamic damping; under the quasi-steady assumption, the tower's aerodynamic damping is given by the following (see Equation (9)): when unsteady effects are included, the tower's aerodynamic damping is calculated as (see Equation (16)). To facilitate the comparison of aerodynamic damping calculation results for the chamfered square tower between the two theories, the aerodynamic damping formulas from both theories are rewritten as functions of the dimensionless wind speed V_*. For the tower's aerodynamic damping calculation under the quasi-steady assumption, the formula can be rewritten as:

$$c_s = \frac{1}{2}\rho v B s = \frac{1}{2}\rho f B^2 s V_* \tag{22}$$

For the tower's aerodynamic damping calculation including unsteady effects, the formula can be similarly rewritten as:

$$c_u = -\frac{1}{2}\rho v^2 (2B) K H_1^* \frac{1}{v} = -2\pi\rho f B^2 H_1^*(V_*) \tag{23}$$

where f denotes the natural frequency of the tower's crosswind vibration. B = 0.1365 m is the characteristic dimension of the sectional model. ρ is the air density, and none of these depend on the galloping theory used. This study defines $c/\left(\rho f B^2\right)$ as the tower's dimensionless aerodynamic damping per unit length c_*, namely:

$$c_* = \frac{c}{\rho f B^2} \tag{24}$$

Therefore, the tower's dimensionless aerodynamic damping under the quasi-steady assumption is calculated as (derived from Equation (22)):

$$c_*{}^s = \frac{1}{2} s V_* \tag{25}$$

When unsteady effects are included, the tower's dimensionless aerodynamic damping is calculated as (from Equation (23)):

$$c_*{}^u = -2\pi H_1^*(V_*) \tag{26}$$

The experiments have measured the galloping coefficient s values and the H_1^*-V_* curves for the chamfered square tower without modifications and after applying two aerodynamic modifications under a 0° wind angle; thus, using Equations (25) and (26), a comparative analysis of the tower's predicted dimensionless aerodynamic damping based on the quasi-steady assumption and including unsteady effects can be conducted, as illustrated in Figure 14. Since galloping occurs only when the aerodynamic damping is negative, the comparison focuses solely on the negative aerodynamic damping predictions from both theories.

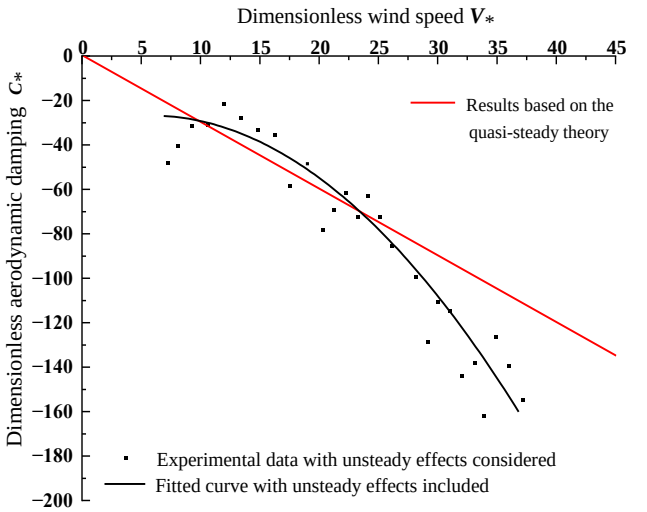

(**a**) Without any modifications

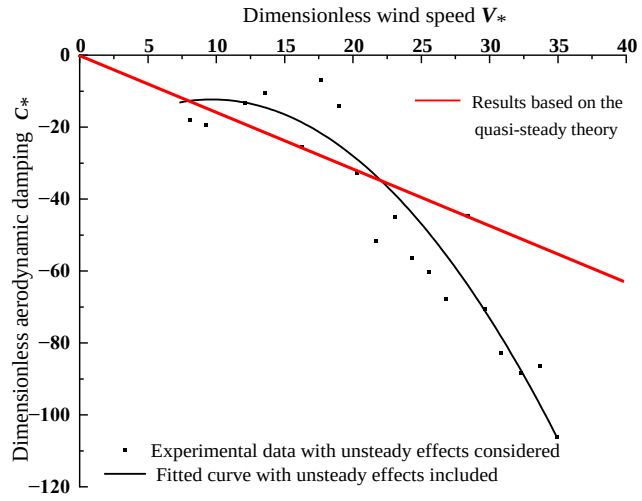

(**b**) With arc-shaped fairings

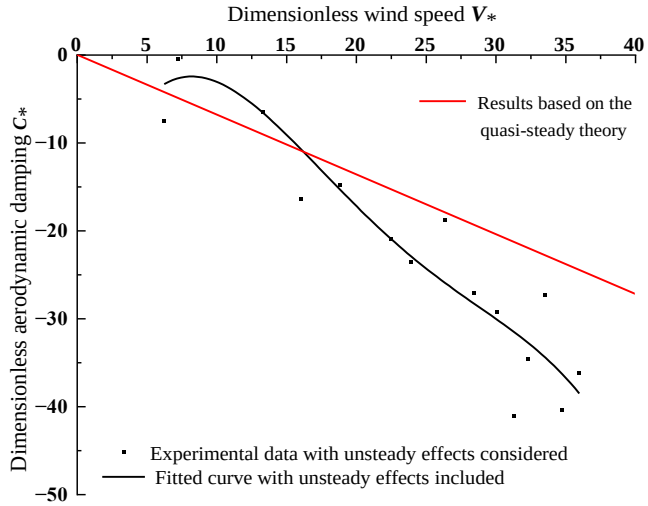

(**c**) With vertical fin plates

Figure 14. Comparison results of aerodynamic damping predicted by two different galloping theories.

The data in the figure reveal that the aerodynamic damping predictions for the chamfered square tower with three different configurations (no modifications, with arc-shaped fairings, and with vertical fin plates) align relatively well between the two galloping theories. However, there are noticeable differences between the two predictions, which are significantly influenced by the dimensionless wind speed. The experimental results for all three tower types generally exhibit the following difference: when the dimensionless wind speed V_* is small, the absolute value of the negative aerodynamic damping predicted by the quasi-steady galloping theory is larger than that from the unsteady galloping theory. When V_* exceeds a certain critical value (or range), the absolute value of negative aerodynamic damping from the quasi-steady theory becomes smaller than that from the unsteady theory. This suggests that, at smaller dimensionless wind speeds V_*, the quasi-steady galloping theory provides a more conservative assessment of the tower's galloping stability compared to the unsteady galloping theory. Conversely, at larger dimensionless wind speeds V_* beyond a certain critical value, the quasi-steady galloping theory offers a more conservative assessment of the tower's galloping stability than the unsteady galloping theory.

5. Conclusions

(1) The conventional tower galloping theory is founded on the quasi-steady assumption, which possesses inherent limitations. By treating tower galloping as a special case of a single-degree-of-freedom lateral bending flutter problem and using flutter derivatives to represent the crosswind aerodynamic forces acting on the tower, unsteady effects induced by motion are incorporated into the galloping analysis. Under these circumstances, the necessary condition for galloping instability in the tower is that the flutter derivative $H_1^* > 0$. For towers susceptible to galloping, the specific critical galloping wind speed can be determined from the H_1^*-V_* (dimensionless wind speed) variation curve.

(2) For the chamfered square tower examined in this study, the galloping coefficient s attains its minimum value at a wind angle of 0°, and it is negative. Regarding the flutter derivative H_1^* of the tower at a 0° wind angle, it transitions to positive values with increasing dimensionless wind speed V_*. Based on the galloping stability criteria from both theories, it is evident that the chamfered square tower may undergo galloping instability at a 0° wind angle.

(3) Installing arc-shaped fairings or vertical fin plates on the chamfered surfaces of the chamfered square tower effectively enhances its galloping stability. This is manifested in the galloping coefficient by markedly increasing the negative s value of the tower, while for the flutter derivatives, it effectively reduces the growth trend of H_1^* in the positive value region.

(4) The experimental results from both galloping theories—based on the quasi-steady assumption and accounting for unsteady effects—exhibit a certain level of consistency. However, some differences are evident, and the disparities between the two theories are considerably affected by the dimensionless wind speed V_*. At smaller dimensionless wind speeds V_*, the quasi-steady galloping theory tends to give a more critical assessment of the tower's galloping stability compared to the unsteady galloping theory; conversely, at higher dimensionless wind speeds V_* beyond a certain critical value (or range), the quasi-steady galloping theory offers a more conservative evaluation of the tower's galloping stability compared to the unsteady galloping theory. These findings are valid for the model tower considered in this study. To generalize the results, additional towers should be tested under the same theories.

Author Contributions: Z.Y.: Conceptualization, Methodology, Investigation, Data curation, Formal analysis, Visualization, Writing—original draft. Y.L.: Conceptualization, Methodology, Validation, Funding acquisition, Writing—review and editing. Y.C.: Funding acquisition, Writing—review and editing. K.D.: Supervision, Validation, Funding acquisition, Writing—review and editing. All authors have read and agreed to the published version of the manuscript.

Funding: This research was funded by the National Natural Science Foundation of China (52108463 and 52278512), Sichuan Science and Technology Projects (2023YFS0427, 2023NSFSC0880 and 2023JDRC0009), and the Chengdu Science Department Project (2022-YF05-00248-SN).

Data Availability Statement: The data presented in this study are available in this article.

Conflicts of Interest: The authors declare no conflicts of interest.

References

1. Sourav, K.; Sen, S. Transition of VIV-only motion of a square cylinder to combined VIV and galloping at low Reynolds numbers. *Ocean Eng.* **2019**, *187*, 106208. [CrossRef]
2. Li, X.; Lyu, Z.; Kou, J.; Zhang, W. Mode competition in galloping of a square cylinder at low Reynolds number. *J. Fluid Mech.* **2019**, *867*, 516–555. [CrossRef]
3. Tamimi, V.; Naeeni ST, O.; Zeinoddini, M.; Seif, M.S.; Dolatshahi Pirooz, M. Effects of after-body on the FIV of a right-angle triangular cylinder in comparison to circular, square, and diamond cross-sections. *Ships Offshore Struct.* **2019**, *14*, 589–599. [CrossRef]
4. Daqaq, M.F.; Alhadidi, A.H.; Khazaaleh, S. Suppression of structural galloping by applying a harmonic base excitation at certain frequencies. *Nonlinear Dyn.* **2022**, *110*, 3001–3014. [CrossRef]
5. Shiraishi, N.; Matsumoto, M.; Shirato, H.; Ishizaki, H. On aerodynamic stability effects for bluff rectangular cylinders by their corner-cut. *J. Wind Eng. Ind. Aerodyn.* **1988**, *28*, 371–380. [CrossRef]
6. Novak, M. Aeroelastic galloping in towers and tall structures. *J. Wind Eng. Ind. Aerodyn.* **1972**, *1*, 189–213.
7. Parkinson, G.; Smith, J. The square prism as an aeroelastic non-linear oscillator. *Q. J. Mech. Appl. Math.* **1964**, *17*, 225–239. [CrossRef]
8. Nishimura, T. Wind tunnel experiments on the aerodynamic forces of rectangular sections. *J. Wind Eng. Ind. Aerodyn.* **2002**, *90*, 123–131.
9. Barrero-Gil, A.; Velazquez, A.; Bécot, F.X. On the galloping instability of bluff bodies: A force–angle analysis. *J. Fluids Struct.* **2009**, *25*, 1296–1308.
10. Barrero-Gil, A.; Sanz-Andrés, A.; Alonso, G. Hysteresis in transverse galloping: The role of inflection points. *J. Fluids Struct.* **2009**, *25*, 1007–1020. [CrossRef]
11. Ng, Y.; Luo, S.; Chew, Y. On using high-order polynomial curve fits in the quasi-steady theory for square-cylinder galloping. *J. Fluids Struct.* **2005**, *20*, 141–146. [CrossRef]
12. Lindner, H. Simulation of the turbulence influence on galloping vibrations. *J. Wind Eng. Ind. Aerodyn.* **1992**, *44*, 2023–2034. [CrossRef]
13. Joly, A.; Etienne, S.; Pelletier, D. Galloping of square cylinders in cross-flow at low Reynolds numbers. *J. Fluids Struct.* **2012**, *28*, 232–243. [CrossRef]
14. Nakamura, Y.; Tomonari, Y. Galloping of rectangular prisms in turbulent flow. *J. Sound Vib.* **1977**, *52*, 233–241. [CrossRef]
15. Parkinson, G.; Sullivan, P. Galloping response of towers. *J. Ind. Aerodyn.* **1979**, *4*, 253–260. [CrossRef]
16. Ruscheweyh, H.; Hortmanns, M.; Schnakenberg, C. Vortex-excited vibrations and galloping of slender elements. *J. Wind Eng. Ind. Aerodyn.* **1996**, *65*, 347–352. [CrossRef]
17. Santosham, T. Force Measurements on Bluff Cylinders and Aeroelastic Galloping of a Rectangular Cylinder. Master's Thesis, University of British Columbia, Vancouver, BC, Canada, 1966.
18. Brooks, P. Experimental Investigation of Aeroelastic Instability of Bluff Two-Dimensional Cylinders. Master's Thesis, University of British Columbia, Vancouver, BC, Canada, 1960.
19. Novak, M.; Tanaka, H. Effect of turbulence on galloping instability. *J. Eng. Mech. Div.* **1974**, *100*, 19–38. [CrossRef]
20. Parkinson, G.V.; Wawzonek, M.A. Some considerations of combined effects of galloping and vortex resonance. *J. Wind Eng. Ind. Aerodyn.* **1981**, *8*, 135–143. [CrossRef]
21. Jones, K.F. Coupled vertical and horizontal galloping. *J. Eng. Mech.* **1992**, *118*, 92–107. [CrossRef]
22. Robertson, I.; Li, L.; Sherwin, S.; Bearman, P. A numerical study of rotational and transverse galloping rectangular bodies. *J. Fluids Struct.* **2003**, *17*, 681–699. [CrossRef]
23. Abdel-Rohman, M. Effect of unsteady wind flow on galloping of tall prismatic structures. *Nonlinear Dyn.* **2001**, *26*, 231–252. [CrossRef]
24. Gao, G.; Zhu, L. Nonlinear mathematical model of unsteady galloping force on a rectangular 2:1 cylinder. *J. Fluids Struct.* **2017**, *70*, 47–71. [CrossRef]
25. Mannini, C.; Massai, T.; Marra, A. Unsteady galloping of a rectangular cylinder in turbulent flow. *J. Wind Eng. Ind. Aerodyn.* **2018**, *173*, 210–226. [CrossRef]
26. Mannini, C.; Marra, A.; Bartoli, G. Vortex-induced vibration and galloping instability of rectangular cylinders in turbulent flow. *J. Wind Eng. Ind. Aerodyn.* **2014**, *134*, 146–160. [CrossRef]
27. Mannini, C.; Marra, A.; Massai, T.; Bartoli, G. Interference of vortex-induced vibration and transverse galloping for a rectangular cylinder. *J. Fluids Struct.* **2016**, *66*, 403–423. [CrossRef]

28. Mannini, C.; Massai, T.; Marra, A. Modeling the interference of vortex-induced vibration and galloping for a slender rectangular prism. *J. Sound Vib.* **2018**, *419*, 493–509. [CrossRef]
29. Liu, Y.; Ma, C.; Dai, K.; El Damatty, A.; Li, Q. Improved understanding of transverse galloping of rectangular cylinders. *J. Wind Eng. Ind. Aerodyn.* **2022**, *221*, 104884. [CrossRef]
30. Sourav, K.; Sen, S. Determination of the transition mass ratio for onset of galloping of a square cylinder at the least permissible Reynolds number of 150. *Phys. Fluids* **2020**, *32*, 063601. [CrossRef]
31. Ziller, C.; Ruscheweyh, H. A new approach for determining the onset velocity of galloping instability taking into account the nonlinearity of the aerodynamic damping characteristic. *J. Wind Eng. Ind. Aerodyn.* **1997**, *69*, 303–314. [CrossRef]
32. Barrero-Gil, A.; Sanz-Andrés, A.; Roura, M. Transverse galloping at low Reynolds numbers. *J. Fluids Struct.* **2009**, *25*, 1236–1242. [CrossRef]
33. Borri, C.; Zhou, S.; Chen, Z. Coupling investigation on VIV and galloping of rectangular cylinders. In Proceedings of the 7th International Colloquium on Bluff Body Aerodynamics and Applications (BBAA7), Shanghai, China, 2–6 September 2012; pp. 2–6.
34. Corless, R.; Parkinson, G. A model of the combined effects of vortex-induced oscillation and galloping. *J. Fluids Struct.* **1988**, *2*, 203–220. [CrossRef]
35. Tian, B.; Cai, M.; Zhou, L.; Huang, H.; Ding, S.; Liang, J.; Hu, M. Numerical simulation of galloping characteristics of multi-span iced eight-bundle conductors tower line system. *Buildings* **2022**, *12*, 1893. [CrossRef]
36. Den Hartog, J. Transmission line vibration due to sleet. *Trans. Am. Inst. Electr. Eng.* **1932**, *51*, 1074–1076. [CrossRef]
37. Scanlan, R.H.; Tomko, J.J. Airfoil and bridge deck flutter derivatives. *J. Eng. Mech. Div.* **1971**, *97*, 1717–1737. [CrossRef]
38. Ma, C.; Liu, Y.; Yeung, N.; Li, Q. Experimental study of across-wind aerodynamic behavior of a bridge tower. *J. Bridge Eng.* **2019**, *24*, 04018116. [CrossRef]